REVISED

Engineering Thiolated Surfaces with Polyelectrolyte Multilayers

*J. D. Delgado, R. L. Surmaitis, Samir Abou Shaheen, and J. B. Schlenoff**
Department of Chemistry and Biochemistry
The Florida State University
Tallahassee, FL 32308 USA
E-mail: schlen@chem.fsu.edu

Keywords: Polyelectrolyte multilayers, adhesion, antifouling, PEGylation, RGD, fibroblasts, gold nanoparticle.

REVISED

ABSTRACT

Interfaces bearing firmly-attached thiol groups are useful for many applications requiring the versatile and facile chemistry of the –SH functionality. In this work, rugged ultrathin films were prepared on substrates using layer-by-layer assembly. The surface of these smooth films was capped with a copolymer containing benzyl mercaptan units. The utility of this coating was illustrated by three applications. First, thiol-ene “click” chemistry was used to introduce the RGD adhesive peptide sequence on a surface that otherwise resisted good adhesion of fibroblasts. This treatment promoted cell adhesion and spreading. Similar Michael addition chemistry was employed to attach polyethylene glycol to the surface, which reduced fouling by (adhesion of) serum albumin. Finally, the affinity of gold for –SH was exploited by depositing a layer of gold nanoparticles on the thiolated surface or by evaporating a tenacious film of gold without using the classical chromium “primer” layer

Introduction

Surface modification is essential in applications for biosensing, catalysis, adhesion, biomaterials and nanotechnology where tailoring the chemical composition of the material interface provides desired properties. The thiol, -SH, group is one of the most versatile functionalities for modifying synthetic and biological surfaces.[1, 2, 3, 4, 5] Thiol chemistries offer a convenient handle for attachment *to* and *from* surfaces. The spontaneous formation of monolayers using the strong interaction of thiol *to* gold has been widely exploited to modify the surface of nanoparticles and planar surfaces.[6, 7, 8] In this case, thiol chemisorption to gold organizes a monolayer coating and more –SH groups per molecule enhance monolayer stability.[9]

Also useful are methods that deposit ultrathin coatings presenting free thiols for further reactions. Such thiolated surfaces include monolayers of dithiols on Au,[6, 7, 10, 11, 12, 13] 3-mercaptopropyltrimethoxysilane for silica,[14, 15, 16, 17] x-ray or electron-induced conversion,[18] multilayering thiolated biomolecules,[19] and modification of surfaces with Grignard reagents and alkanethiols.[20]

Once a thiol is presented at a surface, various methods have been used for further modification, such as Michael-type thiol-ene,[21, 22] radical mediated thiol-ene[23, 24, 25] and thiol-yne addition.[26, 27, 28] These thiol-based “click” reactions provide a powerful approach for engineering multipurpose surfaces. They require mild reaction conditions and they are specific, producing high yields at a fast rate.[29, 30, 31] Recently, much research has focused on Michael addition conjugations, especially those involving the reaction between thiols and electron-deficient maleimides for the immobilization of biomolecules.[32, 33, 34] For example, Houseman et al.[35] demonstrated that SAMs bearing maleimide groups can be used for the fabrication of biochips with thiol-modified ligands. MacBeath et al.[36] used similar features for the preparation of printed microarrays to probe protein–ligand interactions using SAMs with maleimide groups to conjugate ligands containing cysteine to surfaces. Synthetic surfaces usually lack biological functionalities that can be recognized by cells. Therefore, to promote cell adhesion, RGD pendant moieties that mimic cell-extracellular matrix interactions can be incorporated on surfaces[37, 38, 39] for example by coupling thiol and maleimide groups.[40, 41]

While the use of thiol to attach *to* a surface such as Au is relatively straightforward, creating a rugged surface presenting free (“available”) –SH is more demanding. Dithiols, in principle, should yield a monolayer of free –SH if only one thiol attaches to the substrate, but the

spontaneous “lying down” mode of α,ω-dithiols, which is favored for shorter dithiols,[42] consumes both groups. In addition, a layer of clean gold is often not a convenient substrate.[8, 43]

The ideal thiolated surface would have several properties: it could be deposited on a variety of surfaces; it would be persistent, adhere well, offer finely-tuned levels of thiol density, be smooth, remain localized at the surface and offer stability in aqueous and organic solvents. The thiolated surface is implemented here using films of polyelectrolyte complex only a few nm thick deposited by the layer-by-layer assembly method. Biocompatible “multilayers” have been deployed in many biomedical applications.[44] The simplicity and adaptability of this technique provide a versatile platform for surface modification,[45, 46, 47] especially for the control over thickness,[48, 49] hydrophobicity,[50, 51] motility[52] and surface charge.[53]

The present work details the synthesis of a series of polystyrene sulfonate copolymers carrying various levels of protected benzyl mercaptan. When included as the top layer of a polyelectrolyte multilayer, PEMU, the protecting group can be removed, presenting –SH at the surface. The general utility of this thiolated surface was illustrated using three commonly-sought applications for surfaces. First, specific surface-cell interactions were induced by derivatizing thiols with peptides comprising the RGD peptide sequence, known to *promote* specific cell adhesion. Then, thiolated polyelectrolytes were used to enable the attachment of polyethylene glycol, PEG, oligomers, widely used to *prevent* cell adhesion. PEGylation was carried out using thiol-ene click chemistry either before the final layer was deposited on the growing PEMU, or PEG was grafted to thiolated surfaces from solution. Finally, in an “inverted” use of the thiol-Au interaction, Au nanoparticles were spontaneously assembled at the thiolated surface from solution and pure Au film was vacuum evaporated with good adhesion to a thiolated PEMU. These strategies are illustrated in Scheme 1. As it will be shown, this method of producing thiolated surfaces was highly effective.

REVISED

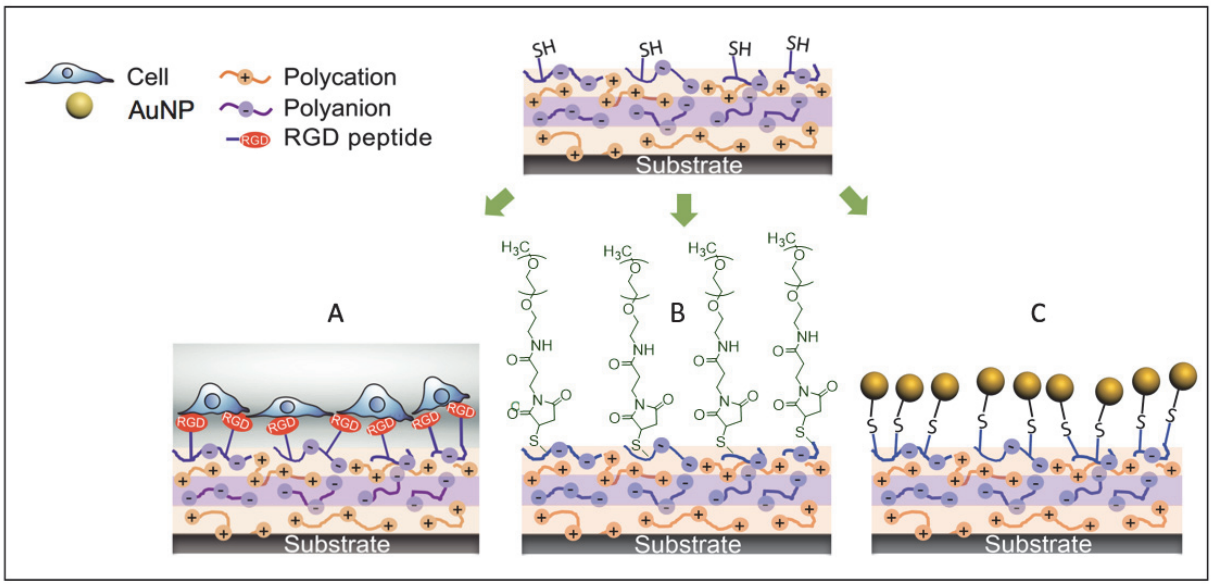

Scheme 1. Applications of substrate-supported ultrathin films bearing a thiolated surface. A. Cell adhesion, B. PEGylation and C. Au nanoparticle adsorption.

Results and Discussion

Synthesis of thiol copolymers

Free radical polymerization in aqueous solutions afforded thiol/styrene sulfonate copolymers. To ensure high molecular weights the thiol group, which is known to participate in chain transfer terminations in free radical polymerization, was protected as the isothiouronium salt ITMS (Supporting Information, Scheme S1). Deprotection occurs under base hydrolysis to form free -SH. This copolymer has been reported previously in a study of the adsorption of poly(styrene sulfonate) to Au.[54]

The compositions of homopolymers and copolymers, determined by size exclusion chromatography and ^{1}H NMR are given in Table 1 (see Supporting Information, Figure S1 and Figure S2 for characterization). It is well known that thiol groups form disulfides under basic conditions in the presence of oxygen. To minimize cross-linking, the proximity of the thiol groups on the polymer backbone was minimized by preparing low loadings of thiol (5, 10 and 15 mol %). Even with lower –SH content the hydrolyzed copolymers slowly crosslinked in solution under ambient conditions. Thus, copolymers were stored in the unhydrolyzed form.

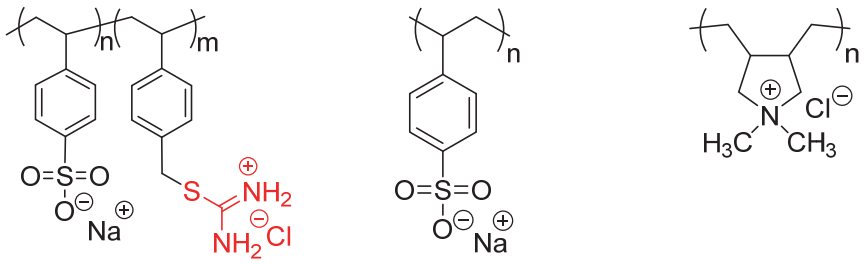

PSS-*co*-PITMS PSS PDADMA

Scheme 2. Structure of polyelectrolytes used in this study.

Table 1. Properties of polyelectrolytes used in this study

Polymer	f[a]	F[b]	Yield (%)	M_w x 10^{-5} (g/mol)[c]	M_w/M_n[c]	d*n*/d*c* (mL/g)[c]
PSS	100	100	-	0.72	2.1	0.175
PDADMA	100	100	-	4 – 5	-	-
PAMS	100	100	-	4.35	1.9	0.163
PSS-**PITMS5%**	5	5.2	40	3.75	1.8	0.173
PSS-**PITMS10%**	10	10.4	47	3.42	1.9	0.172
PSS-**PITMS15%**	15	15.3	51	3.37	2.0	0.171
PSS-**RGD5%**	5	4.8	67	4.34	--	--
PSS-**RGD10%**	10	9.7	70	4.50	--	--
PSS-**RGD15%**	15	15.1	69	4.97	--	--
PSS-**RAD5%**	5	4.7	71	4.36	--	--
PSS-**RAD10%**	10	9.6	68	4.53	--	--
PSS-**RAD15%**	15	14.9	75	5.00	--	--
PSS-**PEG5%**	5	4.6	73	5.38	--	--
PSS-**PEG10%**	10	9.5	68	6.39	--	--
PSS-**PEG15%**	15	14.6	72	7.77	--	--

[a] mole fraction monomer in reaction solution

[b] mole fraction of NaSS and comonomers in polymer determined by ^{1}H-NMR.

[c] Determined bysize exclusion chromatography

M_w of the grafted copolymers were estimated from the M_w of the starting copolymer.

Thiolated surfaces with RGD peptides

Directly prior to the coupling of RGD peptides to copolymers, the protecting group was removed under basic conditions. Figure S2 and S3, Supporting Information shows the kinetics of the deprotecting step of monomer and polymer, respectively, in 10 mM NaOH at room temp. To avoid possible crosslinking due to the formation of disulfide bonds, the hydrolyzed polymer

was maintained in the reduced state by immersion into 10mL of 100mM TCEP.[55] To ensure complete grafting of the copolymer as represented in Scheme 3, a molar excess of the peptide was used. Two peptides were used: *GRGDSP-Maleimide* (**R =** -H) or "RGD" and the control RGD *GRADSP-Maleimide* (**R =** $-CH_3$) or "RAD," which is known to have low specificity for integrins which control cell adhesion (the structures of both peptides are given in Supporting Information Figure S4).[56] The polymers were characterized by ^{1}H NMR (Supporting Information, Figure S5) and size exclusion chromatography (Table 1).

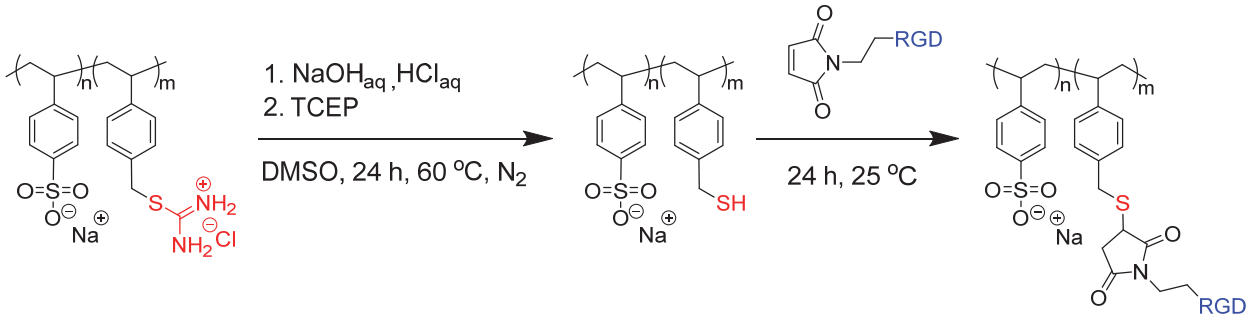

Scheme 3. Synthesis of copolymer containing a RGD sequence (PSS-*co*-RGD). The same grafting procedure was followed for the RAD peptide.

Ultrathin multilayer coatings were deposited on clean silicon wafer substrates or untreated tissue culture plastic well plates (for cell culture experiments). Polyelectrolyte multilayers with a "base" film of 7 layers of PDADMA and PSS (i.e. $[PDADMA/PSS]_3[PDADMA]$) were terminated with a "capping" polymer (CP) which was either PSS, unhydrolyzed copolymer, or copolymer with bound RGD. Multilayers always started with PDADMA on the substrate and are represented by $[PDADMA/PSS,0.15]_3$[PDADMA,0.15][Capping Polymer,1.0], where the number 0.15, 0.5 or 1.0 is the concentration of the salt solution from which the layer was deposited.

These coatings were rugged (they survived immersion in organic solvents and water with NaCl up to 2.5 M), had a total thickness of 11-13 nm and were smooth (rms roughness ca. 2 nm, see Supporting Information Figure S6). Table 2 summarizes the thickness and roughness of the PEMUs with different capping layers. The estimated number of RGD/RAD cm^{-2} was calculated from the capping polymer layer thickness using a density of 1.1 g cm^{-3}.

Table 2. Thickness and roughness of [PDADMA/PSS,0.15]$_3$[PDADMA,0.15][CP,1.0] PEMUs prepared at pH 7.4.

Capping Polymer	Thickness of Base Multilayer (nm)[a]	Thickness of capping (nm)[a]	RMS Roughness (nm)[b]	RGD/RAD[d] x10^{13} cm^{-2}
PSS	9.2	2.5	1.1	-
PSS-*co*-PITMS5%	9.0	2.6	1.5	-
PSS-*g*-RGD5%	8.7	1.9	2.2	2
PSS-*g*-RGD10%	8.8	1.9	2.3	4
PSS-*g*-RGD15%	9.0	2.6	2.5	6
PSS-*g*-RAD5%	9.8	1.7	1.9	2
PSS-*g*-RAD10%	9.0	2.3	2.1	
PSS-*g*-RAD15%	9.2	2.5	2.2	
Silicon wafer [c]	1.5 ± 0.1	-	-	

[a] Dry thickness was measured using ellipsometry ± 0.5 nm.

[b] surface roughness was determined by AFM (5x5 μm^2) ± 0.5 nm.

[c] Native oxide layer.

[d] approximate surface density of ligand

Cells were cultured on [PDADMA/PSS,0.15]$_3$[PDADMA,0.15][capping polymer,1.0] PEMUs for 3 days. When capping polymer = PSS, these multilayers were previously shown to produce nonadhesive surfaces with extra negative charge on [PDADMA/PSS,0.15]$_3$[PDADMA,0.15][PSS,1.0].[57]

Cell adhesion

Cell adhesion is a crucial first step in the cascade of sequences that lead to cell proliferation. Cells bind to adhered proteins in the extracellular matrix via focal adhesions, which are mediated by integrin transmembrane receptors.[58] Extracellular matrix proteins such as fibronectin, contain the peptide sequence Arg-Gly-Asp (RGD) which is a ligand for most integrins.[59] Multilayers have previously been modified with RGD to promote the attachment of a variety of cells, summarized in Table 3.

Table 3. Summary of modified films with RGD used in cell adhesion studies in PEMUs

Surface parameters	Multilayer	Thickness (nm)	Cell type	Capping layer	Capping charge[a]	Reference
pH	PAH/PAA	10 layers	Osteoblast	PAH-RGD	+	[60]
Stiffness	PAH/PAAm	--	Fibroblast	PAH-RGD	+	[39]
pH	PAH/PAAm,PAA	--	Fibroblast	PAH-RGD	+	[61]
	PAH/PAA-PC	--	Fibroblast	PAA-RGD	-	[40]
Stiffness	polylysine/polyglutamate	120	Myoblast	PGA-RGD	-	[37]
Stiffness	polylysine/polyglutamate	31	Osteoblast	PGA-RGD	-	[41]
pH	PAH/PAA	--	Osteoblast	PAH-RGD	+	[62]

The [PDADMA/PSS,0.15]$_3$[PDADMA,0.15][PSS-*co*-RGD5%,1.0] film had a ligand surface density of ca. 2 x 10^{13} molecules cm^{-2} which greatly exceeds the minimum RGD surface density needed to promote fibroblast adhesion, shown to be approximately 5 x 10^9 cm^{-2} (140 nm average spacing).[63] As seen in Figure 1, the RGD-terminated surface is cytophilic, where fibroblasts exhibit a spread morphology covering more area of the culture plastic, whereas the other three comparison surfaces have poorly-attached clusters or aggregates of cells..[57] The spread morphology is a sign of healthy cell adhesion.[64] In the absence of good cell-surface interactions, cell-cell adhesion can dominate, yielding clusters, as seen in Figure 1B,C,D.

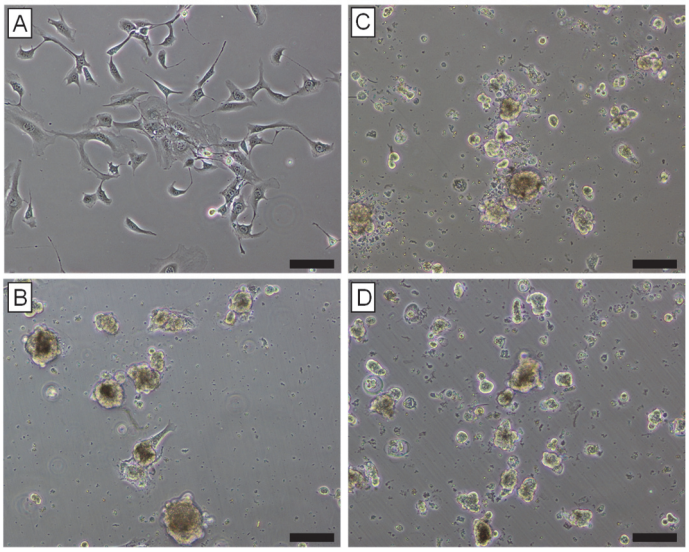

Figure 1. Phase contrast micrographs obtained on day 3 of live 3T3 fibroblasts seeded on [PDADMA/PSS,0.15]$_3$[PDADMA,0.15][capping polymer,1.0] multilayers, where capping polymer = A. [PSS-*co*-RGD$_5$], B. [PSS-*co*-RAD$_5$], C. [PSS-*co*-PITMS$_5$] and D. [PSS]. Scale bar 100 μm.

Thiolated surfaces with PEG

PEGylated surfaces resist protein and cell adhesion. Grafting to polyelectrolytes is one of many techniques used to attach to surfaces. For example, PEG-grafted copolymers of poly(L-glutamic acid), when assembled into multilayers with poly(L-lysine), reduce the adsorption of serum.[65] Wilson et al.[66] used grafted polylysine-*co*-PEG copolymers on PEMUs to eliminate cytotoxicity of polycations. Salloum[45] and Cortez et al.[67] used PSS-*b*-PEG block copolymers on PAH/PSS multilayers to study their antifouling behavior against protein adsorption and cell binding.

Two routes were used to add PEG functionality to the surface of the PEMU. In the first route, the usual base of 3.5 bilayers of PDADMA/PSS was capped by PSS-co-PTMS already grafted with PEG (and fully characterized). The second route involved adsorption of PSS-*co*-PITMS to the surface of the base, followed by hydrolysis then attachment of PEG-mal to –SH by click chemistry. These two routes are represented in Scheme 4. The main point of following these two routes was to verify the efficiency of PEG-mal addition to the surface.

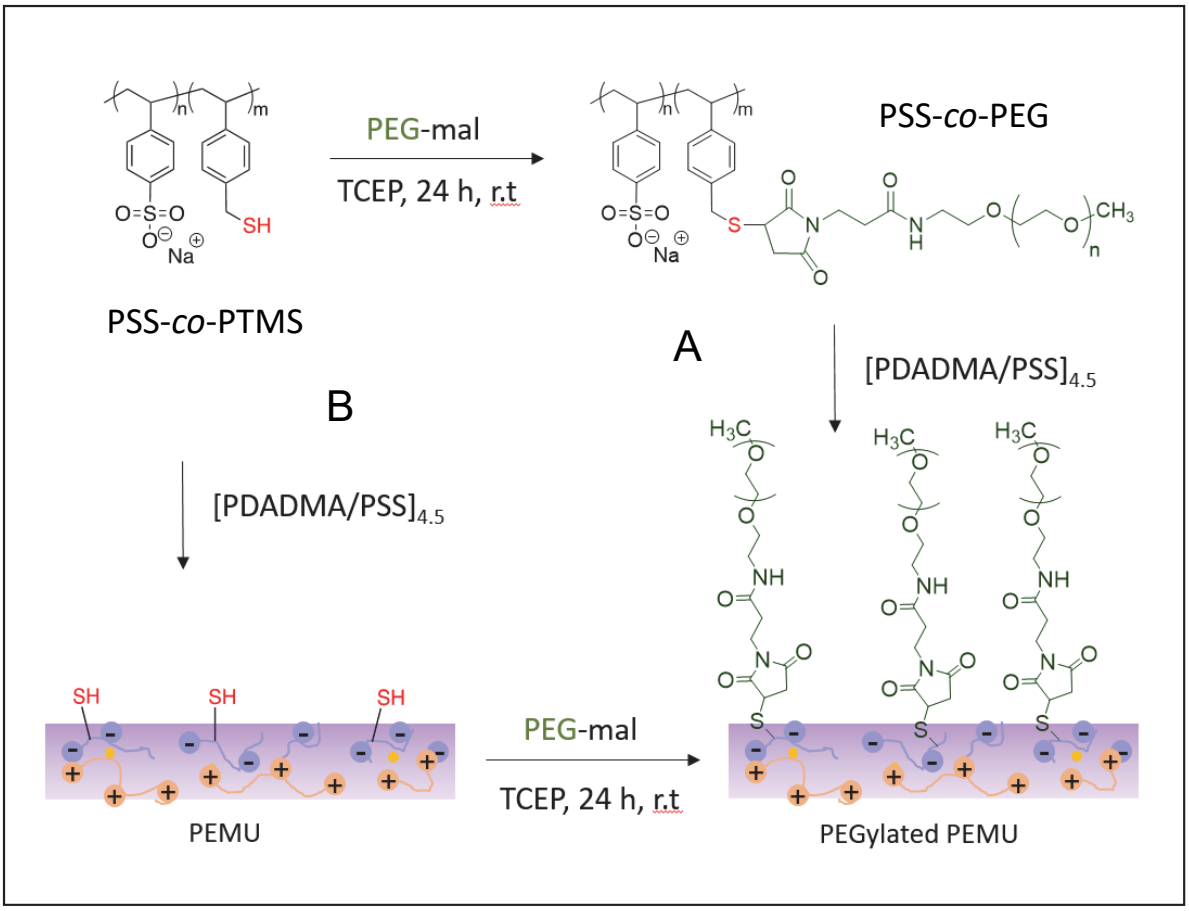

Scheme 4. Routes for including PEG in the capping layer of thiolated copolymer multilayers. A. ROUTE 1 where the copolymer containing PEG (PSS-*co*-PEGX) is premade before assembly and B; ROUTE 2 where the PEG-maleimide is grafted to the thiolated surface.

The grafting efficiency of PEG-mal with PSS-*co*-PTMS having 5, 10 or 15 mol% thiol was determined using ^{1}H NMR. The NMR spectra in Figure S7 indicate quantitative reaction of thiol groups with maleimide, as would be expected for a "click" type reaction. Table 1 summarizes the properties of the copolymers, including the molecular weights of the PSS-*co*-PEG copolymers, which were estimated based on the molecular weight of PSS-*co*-PITMS precursor and grafted PEG chains.

The amount of PEG incorporated into the PEMU surface was determined in two ways. First, the thickness increase of the film provided a semiquantitiative measure of PEGylation.A surface density of 2 x 10^{13} cm^{-2} would give a thickness of about 5 nm of PEG assuming a density of 1.2 g cm^{-3}. Second, transmission FTIR, with subtraction of the signal from the base

layer, gave a more precise result for the composition of the surface. Table 4 summarizes these measurements, including surface roughness (see also the AFM images in Figure S8, Supporting Information). Although the PEG was grafted at a maximum of 15%, the numerous –C-C-O- repeat units provided an adequate signal at around 900 cm^{-1}, seen in Figure 2 (an expanded scale is presented in Figure S9, Supporting Information). The characteristic C-O-C stretch of PEG (1150 - 1050 cm^{-1}) overlaps the $-SO_3^-$ asymmetric stretch from PSS (1190 – 1130 cm^{-1}). The PSS =C-H out of the plane deformation (682 cm^{-1}) and ring in-plane deformation (620 cm^{-1}) are present in all the spectra.

Table 4. Characterization of PEMUs before and after capping with PSS-*co*-PEG

Capping polymer (CP)	[NaCl], M	Thickness of Base Multilayer (nm)[a]	Thickness With Capping (nm)[a]	Capping (nm)[a]	RMS Roughness (nm)[b]	PEG in polymer (%)[c]	PEG in capping layer (%)[d]
PSS-*co*-PEG5%	0.15	9.2 ± 0.3	12.5 ± 0.3	3.3	1.2 ± 0.09	4.8	4.4
PSS-*co*-PEG10%	0.15	9.3 ± 0.3	12.7 ± 0.3	3.4	1.4 ± 0.10	9.7	9.5
PSS-*co*-PEG15%	0.15	9.5 ± 0.3	12.9 ± 0.3	3.4	1.4 ± 0.07	15.1	14.5
PSS-*co*-PEG5%	0.5	22.2 ± 0.3	24.5 ± 0.3	2.3	1.2 ± 0.10	4.7	4.5
PSS-*co*-PEG10%	0.5	22.5 ± 0.3	24.9 ± 0.3	2.4	1.6 ± 0.49	9.6	9.5
PSS-*co*-PEG15%	0.5	22.6 ± 0.3	25.4 ± 0.3	2.8	1.3 ± 0.30	14.9	14.7
PSS-*co*-PEG5%	1.0	44.2 ± 0.3	46.1 ± 0.3	1.9	2.2 ± 0.69	4.6	4.3
PSS-*co*-PEG10%	1.0	44.5 ± 0.3	47.0 ± 0.3	2.5	2.0 ± 0.16	9.5	9.7
PSS-*co*-PEG15%	1.0	44.7 ± 0.3	47.4 ± 0.3	2.7	1.8 ± 0.09	14.6	14.3
Silicon wafer [e]	-	1.5 ± 0.1	-	-	-		-

[a] Dry thickness measured using ellipsometry. ± 1 nm.

[b] Determined by AFM (5x5 μm^2).

[c] Determined by ^{1}H-NMR.

[d] Determined by FTIR by subtracting the base layer.

[e] Native oxide layer.

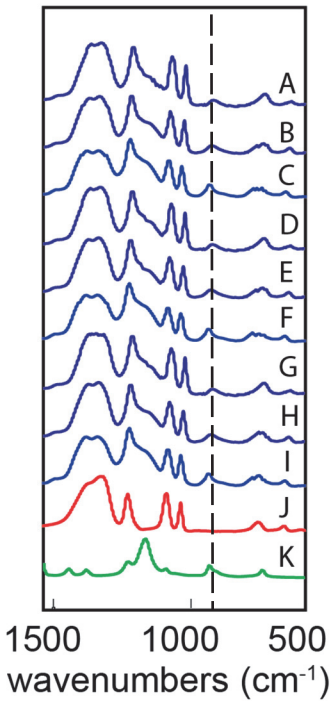

Figure 2. FTIR spectra of [PDADMA/PSS]$_3$[PDADMA][PSS-*co*-PEG**X**] PEMUs, where **X** is the mol% of PEG in the copolymer. (A) PSS-*co*-PEG5% in 0.15 M NaCl, (B) PSS-*co*-PEG10% in 0.15 M NaCl, (C) PSS-*co*-PEG15% in 0.15 M NaCl, (D) PSS-*co*-PEG5% in 0.5 M NaCl, (E) PSS-*co*-PEG10% in 0.5 M NaCl, (F) PSS-*co*-PEG15% in 0.5 M NaCl and (G) PSS-*co*-PEG5% in 1.0 M NaCl, (H) PSS-*co*-PEG10% in 1.0M NaCl, (I) PSS-*co*-PEG15% in 1.0 M NaCl, (J) PSS and (K) PEG.

The ratio of PEG to sulfonate peak areas in Figure 2 was converted to the mol% PEG in the top layer of the multilayer using FTIR spectra of pure component PSS-*co*-PEG copolymers as standards (Supporting Information, Figures S10 and S11) and the peak area ratios of the strong C-C PEG band (960 - 840 cm^{-1}) and the -SO_3^- symmetric stretch of PSS (1036 cm^{-1}) (Supporting Information Table S1 provides detailed peak assignments).

Table 4 shows that the measured PEG surface content matched the expected graft percent. The efficiency of PSS-g-PEG terminated PEMUs in reducing protein adsorption was tested by exposing 5, 10, and 15% PEG capped films to ^{125}I-labeled bovine serum albumin in phosphate buffered saline. Figure S12, Supporting Information, shows that less serum albumin adsorbed on the PEG-capped films than on the control film capped with PSS: the albumin

coverage decreased from 2.5 mg m^{-2} to less than 1 mg m^{-2} (where a monolayer of serum albumin is about 1-2 mg m^{-2}

Following the second route in Scheme 4, PEG was grafted ***to*** the surface after the thiol group was deprotected with a solution of base. PEG-mal was then added to the –SH. In this example of an assessment of the efficiency of a reaction at a surface, the thickness increases and the FTIR adsorption spectra of the multilayer surface (with FTIR of the base subtracted) are shown in Table 5 and Figure 3.). The thickness of PEG provided here by attachment to a dilute population of surface –SH groups was in the range of 2-5 nm, which is about the same thickness as a layer of oligoPEGs.[68]

Table 5. Characterization of PEMUs before and after PEGylation by ellipsometry and AFM.

Capping Polymer	[NaCl] (M)	Thickness of Base multilayer (nm)[a]	Thickness with capping (nm)[a]	Capping (nm)[a]	RMS Roughness (nm)[b]	PEG Grafting (%)[c]
PSS-*co*-PITMS5%	0.15	8.9 ± 0.1	11.8 ± 0.2	2.9	1.2 ± 0.1	4.1
PSS-*co*-PITMS10%	0.15	9.0 ± 0.1	12.5 ± 0.2	3.5	1.4 ± 0.3	9.2
PSS-*co*-PITMS15%	0.15	9.1 ± 0.1	13.5 ± 0.1	4.4	1.3 ± 0.5	14.2
PSS-*co*-PITMS5%	0.5	22.1 ± 0.3	25.4 ± 0.2	3.3	1.2 ± 0.1	3.9
PSS-*co*-PITMS10%	0.5	22.5 ± 0.3	26.0 ± 0.1	3.4	2.3 ± 0.4	9.1
PSS-*co*-PITMS15%	0.5	22.7 ± 0.3	26.3 ± 0.2	3.6	1.5 ± 0.3	14.0
PSS-*co*-PITMS5%	1.0	44.2 ± 0.1	46.5 ± 0.3	2.3	2.9 ± 0.3	4.2
PSS-*co*-PITMS10%	1.0	44.1 ± 0.2	46.6 ± 0.2	2.5	1.9 ± 0.2	9.3
PSS-*co*-PITMS15%	1.0	44.6 ± 0.2	47.4 ± 0.3	2.8	2.3 ± 0.2	14.8
Silicon wafer [d]	-	1.5 ± 0.1	-	-	-	-

[a] Dry thickness measured using ellipsometry.

[b] Determined by AFM (5x5 μm^2).

[c] Determined by FTIR by subtracting the base layer.

[d] Native oxide layer.

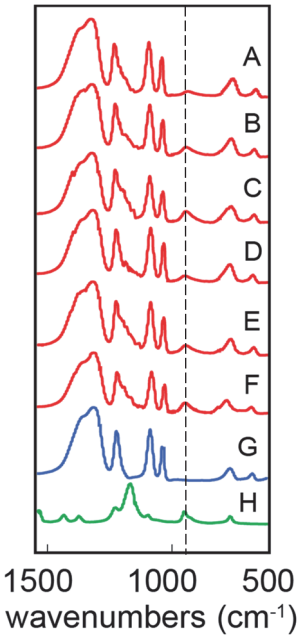

Figure 3. FTIR spectra of [PDADMA/PSS,0.15] PEMUs terminated with PSS-*co*-PEGx, where x is the mol % of PEG in the copolymer: (A) PSS-*co*-PEG5% from 0.5 M NaCl (B) PSS-*co*-PEG10% from 0.5 M NaCl (C) PSS-*co*-PEG15% from0.5 M NaCl (D) PSS-*co*-PEG5% from 1.0 M NaCl (E) PSS-*co*-PEG10% from 1.0 M NaCl (F) PSS-*co*-PEG15% from 1.0 M NaCl, (G) PSS and (H) PEG 300K.

The success of grafting PEG to the thiolated surface allows two important conclusions. First, the thiol functionality remains available for reaction on the surface and does not diffuse into the bulk of the PEMU. In a neutron reflectometry study, Jomaa et al.[69] demonstrated that PSS within a PDADMA/PSS multilayer had a diffusion coefficient on the order of 10^{-17} cm^2 s^{-1} in 0.8 M NaCl. For a dipping time of 15 min this corresponds to a diffusion distance of about 1 nm, suggesting the thiol is essentially "frozen" at the surface. The PSS/PDADMA combination is reasonably strong.[70] Second, although the thiol is bound tightly to the surface, it has enough mobility to react quantitatively with the maleimide (i.e. the "click" reactivity is maintained at the surface).

Thiolated surfaces with AuNP

The assembly of AuNPs on various substrates has attracted much attention, especially for the fabrication of biosensors,[71, 72, 73] where it was found to improve the sensitivity of devices due to their plasmonic characteristics. Biosensing techniques such as surface-enhanced Raman

spectroscopy,[74, 75, 76] benefit from nanostructuring of Au at the interface. Theoretically, a smooth thiolated surface should be capable of spontaneously collecting AuNPs from solution, especially if they are stabilized with weak ligands.

The citrate stabilized AuNPs prepared in this work were estimated by dynamic light scattering to have an average hydrodynamic diameter of 17.1 nm (Supporting Information, Figure S13). The AuNP concentration in solution was estimated by the AuNP absorption and its diameter to be around 1.54 nmol L^{-1}. To establish the feasibility of adsorbing AuNPs to the surface the copolymer with highest concentration of -SH groups (PSS-*co*-PITMS**15%**) was used.

PEMUs capped with PSS-*co*-PITMS**15%** were built on two substrates: a quartz cuvette allowed the UV-vis absorption spectrum to be monitored in the wavelength range from 200 to 800 nm. Si wafers were used as substrates for the SEM analysis. The terminal amidinothio protecting groups in the top layer were converted into thiols by reaction with NaOH then TCEP prior to AuNP immersion. As a control, $[PDADMA/PSS, 0.15]_4$ was treated in the same way then exposed to AuNPs under the same conditions. To remove loosely bound nanoparticles, the films were rinsed with pure water

UV−vis spectra of the PDADMA/PSS PEMU taken after each of the first 3 bilayers show the regular growth of the PSS absorption band at 240 nm (Supporting Information, Figure S14). The capping layer also shows the growth of this band, as well as a weak absorption at about 580 nm, attributed to a layer of adsorbed AuNPs. This peak is magnified in Figure 4 and compared to the absorption spectrum from the citrate capped AuNPs suspended in solution. There is a red shift in the plasmon band of the Au on the surface due to interactions between the AuNPs.

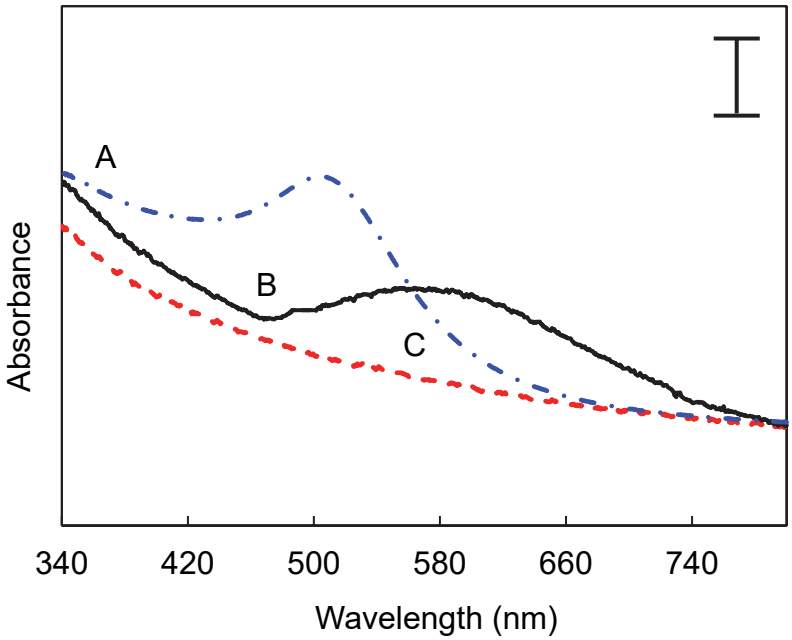

Figure 4. UV-vis absorption spectra of (A) (–·–) AuNP capped with citrate in solution, (B) (**–**) [PDADMA/PSS 0.15]$_{3.5}$[PSS-*co*-PITMS15% 0.15] decorated with adsorbed AuNP and; (C) (---) [PDADMA/PSS 0.15]$_{3.5}$[PSS-*co*-PITMS15% 0.15] control multilayer. Scale bar corresponds to A: 0.17 AU; B and C: 0.012 AU.

Scanning electron microscopy was also used to demonstrate the affinity of thiolated surfaces to AuNPs. Coated Si wafers were dipped into a solution of citrate-capped AuNPs and rinsed. The SEM images shown in Figure 5 depict the starting [PDADMA/PSS 0.15]$_{3.5}$[PSS-*co*-PITMS15% 0.15] multilayer and one after hydrolysis then adsorption of AuNPs, where the nanoparticles are clearly seen to decorate the surface in a packed morphology.The shift in plasmon resonance in Figure 4 is consistent with the dense packing seen in Figure 5C. A more dilute coverage of thiol might yield separated nanoparticles. Polymer-on-polymer stamping[77] with a pattern inked with the thiol copolymer would provide specific micropatterned areas for Au nanoparticle adhesion. A [PDADMA/PSS 0.15]$_4$ control surface adsorbed no nanoparticles when immersed in the AuNP solution (Figure 5).

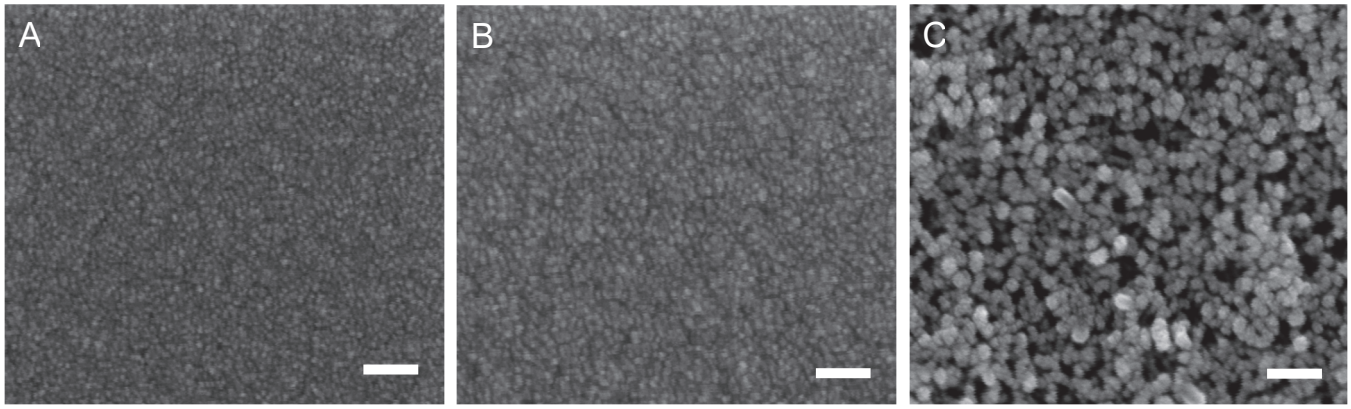

Figure 5. SEM images of (A) [PDADMA/PSS 0.15]$_{3.5}$[PSS-*co*-PITMS15% 0.15], (B) [PDADMA/PSS 0.15]$_4$ + AuNP and (C) [PDADMA/PSS 0.15]$_{3.5}$[PSS-*co*-PTMS15% 0.15] + AuNP. Scale bars are 100 nm.

Adhesion of evaporated Au

As a final test of the versatility and utility of the thiolated surface it was used to enhance the adhesion of evaporated Au film to glass. Evaporated Au films, widely used as electrodes, usually require a thin intermediate layer of Cr or Ti in order to adhere to glass or silica. Goss et al.[78] reported the use of mercaptopropyltrimethoxysilane as an alternative priming layer, where the (hydrolyzed) silane condenses on glass therefore presenting –SH at the surface. In the present work, a clean, glass microscope slide was hydrolyzed in NaOH then Au was evaporated directly onto the film. At the same time Au was evaporated onto PSS-terminated multilayer coated glass and PSS-*co*-PTMS15%-terminated multilayer coated glass. Peel tests with tape removed all Au coated onto glass except for the section that was coated with a multilayer of PTMS15%-terminated film, as seen in the photographs in Figure 6.

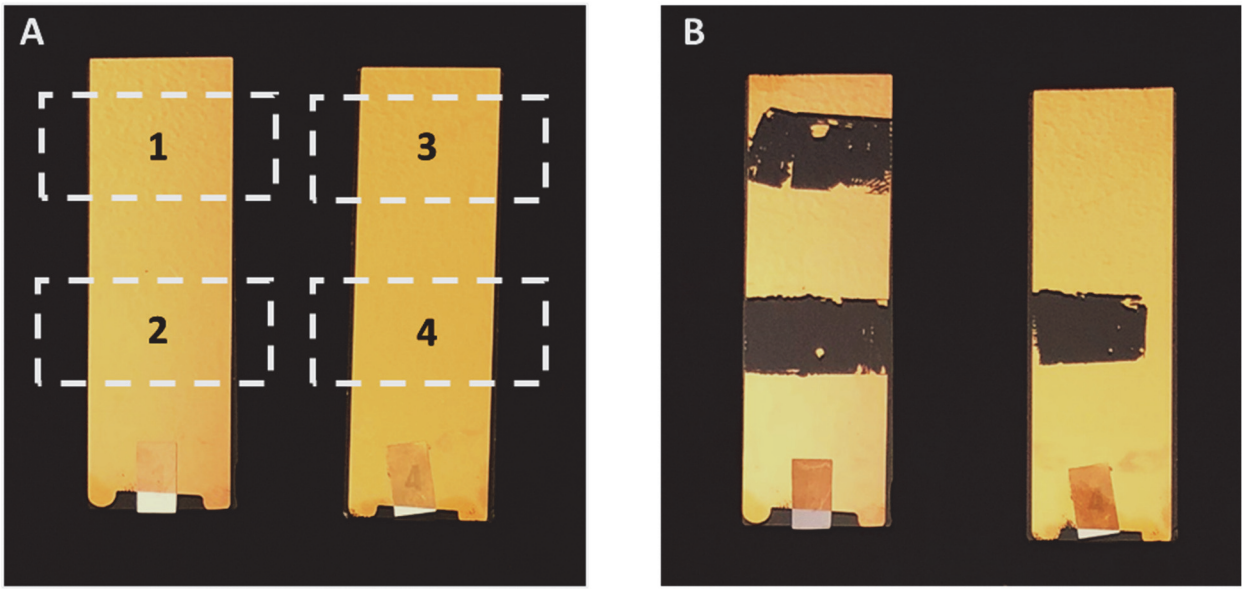

Figure 6. Peel test on gold coated PEMUs. (A) Samples before applying adhesive tape and (B) Samples after peeling off the adhesive tape. Dashed lines show where the tape was applied and the numbers 1-4 correspond to regions terminated in: 1. PSS, 2. Uncoated glass 3. PSS-*co*-PTMS15% and 4. PSS-*co*-PITMS15% respectively. Only area 3, which contains the deprotected thiol, prevents stripping of the gold by the tape.

Conclusions

The ultrathin films described here, made from multilayered polyelectrolytes and falling in the range 15 – 45 nm, fulfill many of the requirements for a general, practical, reactive surface modification technique. Although these multilayers are only a few nm thick they provide a rugged platform for presenting accessible thiol functionality which then serve as attachment points using well-known and efficient chemistry. Maleimide-terminated adhesive peptides or PEG were used to show respective applications as cell adhesive and protein resistant coatings. The affinity of -SH for Au promoted the adhesion of gold nanoparticles or gold film. Assemblies of gold nanoparticles are of interest for plasmonics applications and as substrates for surface enhanced Raman sensors. Gold film is used extensively in the electronics industry but on most substrates it must be primed with an intermediate adhesion layer of chrome or titanium. Since multilayers may also be deposited on nanoparticles of any shape it is anticipated that the thiol capped films described here could also be used at the interface between particle and continuous phase for nanocomposites.

Experimental

Materials. Sodium 4-vinylbenzenesulfonate (NaSS, purity ≥ 90%, Sigma-Aldrich) was recrystallized from water to a monomer purity of > 98%; 4-vinylbenzyl chloride (90%, Acros organics), and poly(diallyldimethylammonium chloride) (PDADMA, M_w 400,000-500,000 g mol^{-1}, 21.5% in water, Sigma-Aldrich) were used as received. Poly(sodium 4-styrenesulfonate) (PSS, M_w 70,000 g mol^{-1}, Scientific Polymer Products), was purified by dialysis (Spectra/Por dialysis tubing, molecular weight cutoff = 12,000-14,000) and then dried by lyophilization. 2,2′-Azobis(2-methylpropionitrile) (98%, Sigma-Aldrich) initiator,) was recrystallized twice from methanol. Deuterated dimethyl sulfoxide (Cambridge Isotope Laboratories, Inc.), cosmic calf serum (Thermo Scientific), PEG-maleimide (PEG-mal, M_w 2,000 g mol^{-1}, Creative PEGWorks), PEG (M_w 300,000 g mol^{-1}, Sigma-Aldrich) and tris(2-carboxyethyl)phosphine hydrochloride (TCEP, ≥ 98%, BIOSYNTH) were used as received. The peptide sequences GRGDSP-maleimide (HPLC purity ≥ 96.4%, M_W = 738.71 g mol^{-1}) and GRADSP-maleimide (HPLC purity ≥ 96.3%, M_W = 752.74 g mol^{-1}) were provided by GenScript. 3T3-Swiss albino fibroblasts were initially purchased from American Type Culture Collection as ATCC CCL-92 cells and maintained in the laboratory for numerous generations. Gentamicin (Invitrogen), Trizma® base (Sigma-Aldrich, ≥ 99%), Trizma® hydrochloride (Sigma-Aldrich, ≥ 99%), thiourea (Sigma-Aldrich, ≥ 99%) NaCl (Sigma-Aldrich, ≥ 99.5%), $Na_3C_6H_5O_7$ (Sigma-Aldrich, ≥ 99.5%), $NaBH_4$ (Sigma-Aldrich, ≥ 99%), and chloroauric acid trihydrate ($HAuCl_4 \cdot 3H_2O$, ≥ 99.9%, Sigma-Aldrich), were used as received. Deionized water (18 MΩ cm, Milli-Q) was used to prepare aqueous solutions. All cell experiments were carried out on flat bottom, 12-well untreated polystyrene plates (Jet-Biofil).

Synthesis of 4-[(amidinothio)methyl]styrene hydrochloride (ITMS). The thiolated monomer ITMS was made following a literature method:[57] 4-vinylbenzyl chloride (15.3 g, 0.1 mol), and thiourea (9.12 g, 0.12 mol) were dissolved in 200 mL of 1:1 ethanol and acetone. The mixture was stirred at 30 °C for 24 h under nitrogen. The solution was cooled to r.t. and concentrated under vacuum. The product was transferred into a large amount of diethyl ether and the white precipitate collected and washed 3 times with diethyl ether and dried under vac. ^{1}H NMR (600 MHz, DMSO-d_6) δH in ppm: 4.51 (s, 2H, CH2-S), 5.30 [d, 1H, CH2=CH (trans)], 5.86 [d, 1H, CH2 = CH (cis)], 6.72 [dd, 1H, CH2=CH (gem)], 7.41 (d, arom-CH), 7.48 (d, arom-CH), and 9.32 (s, 4H, isothiouronium). ^{13}C NMR (600 MHz, DMSO-d_6) δC in ppm: 34.28 (CH2-S), 114.92 (CH2=CH), 126.55 and 129.40 (arom-CH), 133.91 and 1336.09 (arom C), 136.84 (CH2=CH), and 169.55 (C-isothiouronium). (Supporting Information, Figure S1).

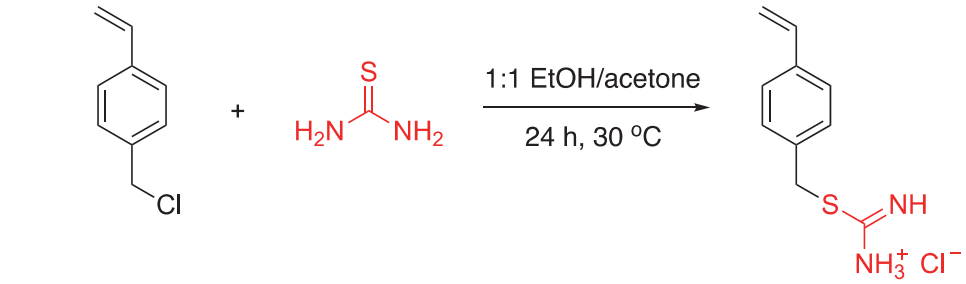

Scheme 2. Synthesis of the amidinothio protected monomer (ITMS).

Polymerization of 4-[(amidinothio)methyl]styrene hydrochloride (PITMS). ITMS (2 g) and 0.1 g of initiator were dissolved in 10 mL of DMSO under nitrogen. Polymerization was carried out at 70 °C. The product was cooled and dialyzed against water (using Spectra/Por 12,000 - 14,000 molecular weight cutoff tubing) for 40 h. The purified polymer was freeze-dried as a white powder (90% yield). The disappearance of the vinylic protons and the presence of the new aliphatic protons at about 2 ppm was observed by ^{1}H NMR. ^{13}C NMR (DMSO-d_6): 6 34 (-CHI, 114.8 (CH_2=), 125.6 and 126.5 (CH=ring), 135.5 and 136.0 (-C= ring), 169.2 (>C=NH).

Poly(4-styrenesulfonate-co-4-[(amidinothio)methyl]styrene)(PSS-co-PITMS15%). NaSS (2.2 g, 1.1 mmol) and the amidinothio salt ITMS (0.44 g, 0.17 mmol) were dissolved in 10 mL of DMSO. Polymerization was carried out under nitrogen using initiator at 60 °C. The polymer was purified by dialysis against water and recovered by freeze-drying to yield a white product (47 % yield). ^{1}H NMR (DMSO-d_6, 600 MHz): (Supporting Information, Figure S2).

Deprotection of the amidinothio group. PSS-*co*-PITMS15% (1.0 g, 4.77 mmol) was dissolved in 10 mL water under nitrogen, then the pH was adjusted to 12 with 1M NaOH. The solution was stirred at room temp for 2 h. The reaction was quenched with excess dil HCl_{aq} and the solution was stirred for 5 min until a pH of about 7 was obtained. The product was purified by dialysis against dil HCl pH = 3.4 and then pure water using Spectra/Por tubing. The deprotected copolymer was recovered by freeze-drying. (87 % yield). ^{1}H NMR (DMSO-d_6, 600 MHz): (Supporting Information, Figure S2).

PSS-co-RGD15%. PSS-*co*-PTMS15% (0.1 g, 0.5 mmol) was dissolved in 10 mL DMSO followed by the addition of TCEP, (30 mg, 0.1 mmol). The reaction flask was subjected to 3 freeze pump thaw cycles to remove O_2 then heated at 60 °C for 2 days. After cooling to r.t; RGD-maleimide (0.1 mmol) dissolved in 5 mL of DMSO was added dropwise to the solution. After the reaction mixture was stirred for an additional 24 h at room temp, methanol was added

to precipitate the polymer. The product was collected by filtration, dissolved in water, and dialyzed against water (Spectra/Por 12,000 - 14,000 molecular weight cutoff tubing) for 40 h. The purified polymer was freeze-dried (75% yield) and stored at -23 ^{o}C. ^{1}H NMR (DMSO-d_6, 600 MHz): (Supporting Information, Figure S2). PSS-co-RAD15% was prepared in the same way.

PSS-co-PEG15 %. PSS-*co*-PTMS15% (0.1 g, 0.5 mmol) was dissolved in 10 mL of DMSO followed by the addition of TCEP, (30 mg, 0.1 mmol) and heated at 60 ^{o}C for 2 days. PEG-maleimide (0.2 g, 0.1 mmol) in 10 mL 50/50 DMSO/H_2O was added to the mixture then stirred under nitrogen at room temp for 24 h. The product was dialyzed against water then freeze-dried (81 % yield). Supporting Information, Figure S3 shows ^{1}H NMR (D_2O, 600 MHz) spectra of PSS, PEG homopolymers and PSS-*co*-PEG copolymers. In the PSS-*co*-PEG spectrum, the resonance band observed at 0.8 – 2.2 ppm. is attributed to the backbone protons of the PSS, and the composition of PEG in the copolymers was determined from the intensity ratio of the resonance of the phenyl protons of PSS at 6.2–7.8 ppm, and the PEG main chain protons at 3.7 ppm.

Growth of gold nanoparticles. Citrate stabilized AuNPs (R_D ~ 17 nm as measured by dynamic light scattering) were synthesized according to Turkevich et al.[79] In brief, $HAuCl_4 \cdot 3H_2O$ (50 mM, 5 mL) was added to a boiling aqueous solution of sodium citrate (1.7 mM, 500 mL) The reaction was allowed to proceed until the solution attained a wine red color and left under vigorously stirring for 15 min. The mixture was then cooled to room temperature. The gold nanoparticles were purified using a centrifugal filtration device (Millipore, MW cutoff = 50 kDa).

Polyelectrolyte multilayer buildup. Polyelectrolyte solutions of concentration 10 mM (based on the repeat unit) were made in 0.15, 0.5 and 1.0 M NaCl. For thickness measurements, multilayers were built using 1000 mL beakers and a holder with a capacity for 6 double side polished wafers (Okmetic, 381 ± 12 µm thick, 125 ± 0.5 mm diameter). The Si wafers were cleaned in “piranha” (70% H_2SO_4/30% H_2O_2, *Caution! Piranha solution is very corrosive and extreme care should be taken when handling*) for 15 min at room temp then washed vigorously with water and dried under a N_2 stream. To make multilayers on Si wafers they were attached vertically to a stainless-steel shaft and rotated at 300 rpm. The dipping time of each of the polymer solutions was 15 min which was followed by 3 x (1 min) rinsing steps in deionized water.

Polyelectrolyte multilayers on tissue culture plastic. Cell culture experiments were performed on PEMUs prepared using the LbL technique on tissue culture plastic plates. Tissue culture plastic plates were clean, sterile and sealed. During the build-up the plates were immersed completely into 1000 mL beakers containing polyelectrolyte solution. After

completion, the plates were dried at room temp and the cell seeding was done less than 24 h after the film was made.

PEMU nomenclature. $[PDADMA/PSS,x]_n$ multilayers, where n indicates the number of bilayers and x the concentration of NaCl that was used for the build-up. For example: $[PDADMA/PSS,0.15]_3$[PDADMA,0.15][CP,1.0] indicates 6 alternating layers of PDADMA and PSS, starting with PDADMA on the Si wafer, using 0.15M NaCl in both polyelectrolyte solutions and the last polyelectrolyte layer added or capping polymer, from 1.0 M NaCl. For this study capping polymer = PSS, PSS-co-PITMSX, PSS-*co*-RGDX, PSS-*co*-RADX or PSS-co-PEGX with X = 5, 10 or 15 mol %.

Cell culture. 3T3-Swiss albino fibroblasts were cultured in Dulbecco's Modified Eagle's medium supplemented with 1 g L^{-1} L-glutamine, 1.2 g L^{-1} $NaHCO_3$,10% cosmic calf serum, 100 U mL^{-1} penicillin G, 100 µg mL^{-1} streptomycin, 0.25 µg mL^{-1} amphotericin B, and 10 µg mL^{-1} gentamicin. Cells were incubated at 37 °C with 5% CO_2 (Nu-4750, NuAire). Uncoated 6- or 12-well plates were used as controls.

Conjugation of PEG-maleimide (PEGylation) to PEMUs. For the PEGylation of the PEMUs the $[PDADMA/PSS, 0.5]_{3.5}$[PSS-*co*-PITMS15%,0.5] film was immersed in 10 mL $NaOH_{aq}$ at pH 12 and stirred gently for 2 h at room temp. To reduce any disulfide bonds that may have formed at the monolayer, PEMUs were immersed in a 10 mL 100 mM TCEP for 10 min at room temp, followed by the three water rinses. To carry out the thiol-ene chemistry the PEMU was immersed in 10 mL 50 mM PEG-maleimide solution under stirring. After 24 h, the substrate was rinsed with water and dried under a stream of nitrogen. As a control, $[PDADMA/PSS, 0.5]_4$ was also reacted with PEG-maleimide under the same experimental conditions.

Conjugation of AuNP's to PEMUs. In a similar way to the PEGylation procedure, the deprotection and exposure of thiol groups on PEMUs was carried out by immersing $[PDADMA/PSS, 0.15]_{3.5}$[PSS-*co*-PITMS15%,0.15] in a solution of NaOH at pH 12, then a TCEP solution, followed by the three water rinses. The film was immersed in a solution of freshly prepared AuNPs. After 24 h, the substrate was carefully rinsed with water and dried under a stream of nitrogen. As a control, $[PDADMA/PSS, 0.15]_4$ was also reacted with the AuNP's under the same experimental conditions.

Microscopy and live cell imaging. Fixed cell images were collected with a Nikon TS100 microscope fitted with a Nikon DS-Ri1 camera. Live cells were imaged with a Nikon Ti-E inverted microscope and a Cool Snap HQ2 camera. Cells were housed in a LiveCell chamber

(Pathology Devices), incubated at 37 °C and monitored for 72 h in 5% CO_2. 60% relative humidity was used to reduce media evaporation.

^{1}H NMR. Copolymers were analyzed by ^{1}H-NMR (Avance-600 MHz, Bruker), where all chemical shifts for ^{1}H NMR spectra are reported relative to tetramethylsilane in the deuterated solvent. The ITMS composition in PSS-*co*-PITMS copolymers was calculated from the integrated areas of NaSS and ITMS.

Sample preparation. All solutions used in size exclusion chromatography, SEC, were prepared by dissolving the required amount of dried polymer in the salt solution. All the polymers for use in light scattering measurements and refractometry were dried under vacuum and weighed in an Ar-filled dry box.

Size exclusion chromatography. Absolute number-average molar mass (M_n), weight-average molar mass (M_w), and polydispersity ($D = M_w/M_n$) of polymers were determined using size exclusion chromatography with three 17 μm columns (30 x 7.5 mm, Tosoh Biosciences TSK-GEL G5000PW) in series with a TSK guard column, then a DAWN-EOS light scattering detector (λ = 690 nm) previously calibrated with toluene and an OPTILAB-REX interferometric refractometer, both from Wyatt Technologies. The concentration of polymer solution injected was 2.5 mg mL^{-1} in 0.3 M $NaNO_3$ and the mobile phase was 0.3 M $NaNO_3$ at a flow rate of 1.0 mL min^{-1}. All mobile phases were maintained at 25 ˚C. Poly(sodium 4-styrenesulfonate) standards from Scientific Polymer Products Inc. were used to check the performance of the instrument. Detectors at various angles were normalized with bovine serum albumin. Data were analyzed using ASTRA 6.1 software from Wyatt technology. The specific refractive index increment, *dn/dc*, was determined on the OPTILAB-REX.

Dynamic light scattering. Dynamic light scattering experiments were performed using a goniometer system (ALV CGS-3-A0-111, Langen, Germany), with a laser (λ = 632.8 nm) with vertically polarized light and a power of 22 mW. Measurements were made at an angle of 90^o and a temperature of 25.0 ^{o}C in 10 mm dia. cylindrical borosilicate glass tubes through a cylindrical reservoir which was filled with a refractive index matching liquid (toluene). All AuNP solutions were filtered through 0.2 μm syringe filters (Millipore). The autocorrelation function was the average of three runs of 10 s each. The intensity autocorrelation function $g_2(q,\tau)$ where $q = 4\pi n_D \sin(\theta/2)/\lambda$ was obtained by pseudo-cross-correlation of the signals from two photomultipliers to suppress noise using ALV-correlator software V.3.0. The hydrodynamic radius (R_h) was calculated from the measured diffusion coefficient using the Stokes-Einstein relationship (Eq. 1):

$$R_h = \frac{k_B T}{6\pi\eta D} \quad (1)$$

where k_B is the Boltzmann constant, T is the absolute temperature, and η is the solvent viscosity. Since D is an average translational diffusion coefficient, R_h represents the average hydrodynamic radius of nanoparticles in solution. Distributions in R_h were calculated using CONTIN analysis.

Film thickness. All multilayers were built at room temp (23 ± 2 °C). Film thicknesses were measured with an ellipsometer (Gaertner L116S, Gaertner Scientific Corp.), using 632.8 nm light at a 70° incidence angle. A refractive index of 1.55 was used for multilayers.

Fourier transform infrared (FTIR) spectroscopy. FTIR spectra of PEMUs were obtained with a Thermo Avatar 360 equipped with a DTGS detector at a resolution of 4 cm^{-1} with 100 scans. The background was obtained using an uncoated Si wafer. EZ-OMNIC software was used to analyze the spectra and calculate peaks area.

UV-vis spectroscopy. UV-vis absorption measurements were carried out using a UV 2450 absorption spectrophotometer (Shimadzu). Polyelectrolyte solutions were made in 0.15 M NaCl. Multilayers were built up using a quartz cuvette (d = 1 cm) cleaned in "piranha." The dipping time of each of the polymer solutions was 5 min which was followed by 3 x (1 min) rinsing steps in deionized water, yielding PEMUs that were monitored by UV-vis spectrophotometry in the wavelength range from 200 to 800 nm.

Radiolabeling assay. $Na^{125}I$ (1 mCi, PerkinElmer), supplied in 10 µL 1.0 x 10^{-5} M NaOH, was mixed with 1.0 mL of PBS and added to 2.0 mL of 1.0 mg mL^{-1} of unlabeled bovine serum albumin (Sigma Aldrich). Three iodination beads (Thermo Scientific) were added to iodinate the protein. 7.0 mL of PBS was added to the 3.0 mL [^{125}I]-bovine serum albumin solution to make 10.0 mL of 0.2 mg mL^{-1} [^{125}I]-bovine serum albumin solution with a specific activity of about 0.5 mCi mg^{-1}. This solution was filtered using a 0.1 µm filter then dialyzed (Thermo Scientific, Dialysis cassette, molecular weight cutoff=3,500) for 12 h. PEMUs for albumin deposition were built on Si wafers. A lead spacer with a fixed area (0.5 cm^{-2}) of exposure to the scintillator was placed between the wafer and the scintillator (EJ-256-5 Elgen Technology, 6.35 mm thick, 25.4 mm diameter, emission peak 425 nm) to keep the area in view of the photomultiplier tube window constant. A calibration curve (cps vs. µg of [^{125}I]-bovine serum albumin) was constructed by depositing increments of 1.0 µL of radiolabeled solution on the scintillator. The Si wafer was then placed on the scintillator on the PMT window. Supporting Information, Figure S15 shows how µg of added serum albumin were converted to mg m^{-2} using the area of the exposed film.

Atomic force microscopy (AFM). The dry surface roughnesses of PEMUs were determined using an MFP-3D atomic force microscope (Asylum Research Inc.) equipped with an ARC2 controller. NCHV probes from Bruker (tip radius = 8 nm, spring constant 20 – 75 N m^{-1}) were used at a scan rate of 0.5 Hz. Images of 20 × 20 μm and 5 × 5 μm scan ranges were collected and then analyzed using Asylum Research software. Roughness was obtained from 5 × 5 μm regions at different positions of 20 x 20 μm images.

Scanning electron microscopy (SEM). Experiments were carried on a FEI Nova NanoSEM 400 set at 10 kV with a working distance of 5 mm. High magnification was attained using the through-the-lens detector with field immersion mode. Before imaging, samples were coated with a 4 nm-layer of iridium using a Cressington HR 208 sputter coater.

Supporting Information

NMR spectra of monomers and hydrolysis of ITMS; NMR spectra of amino acids conjugated to polyelectrolytes; AFM images of multilayer surfaces; FTIR spectra of multilayers; adsorption of radiolabeled albumin on surfaces; calibration curve for albumin adsorption; dynamic light scattering of AuNPs.

Acknowledgments

This work was supported in part by a grant from the National Science Foundation (DMR-1506824), and by the Florida State University. We gratefully acknowledge Hadi Fares for the SEM analysis and Dr. Banghao Chen for help with NMR.

REFERENCES

1. Chen, Y.-S.; Choi, H.; Kamat, P. V. Metal-Cluster-Sensitized Solar Cells. A New Class of Thiolated Gold Sensitizers Delivering Efficiency Greater Than 2%. *Journal of the American Chemical Society* **2013,** *135*, 8822-8825.
2. Ford, M. J.; Masens, C.; Cortie, M. B. The Application of Gold Surfaces and Particles in Nanotechnology. *Surface Review and Letters* **2006,** *13*, 297-307.
3. Jain, P. K.; Qian, W.; El-Sayed, M. A. Ultrafast Cooling of Photoexcited Electrons in Gold Nanoparticle−Thiolated DNA Conjugates Involves the Dissociation of the Gold−Thiol Bond. *Journal of the American Chemical Society* **2006,** *128*, 2426-2433.
4. Madaan, N.; Terry, A.; Harb, J.; Davis, R. C.; Schlaad, H.; Linford, M. R. Thiol–Ene–Thiol Photofunctionalization of Thiolated Monolayers with Polybutadiene and Functional Thiols, Including Thiolated DNA. *The Journal of Physical Chemistry C* **2011,** *115*, 22931-22938.

5. Pavlovic, E.; Oscarsson, S.; Quist, A. P. Nanoscale Site-Specific Immobilization of Proteins through Electroactivated Disulfide Exchange. *Nano Letters* **2003,** *3*, 779-781.
6. Bain, C. D.; Troughton, E. B.; Tao, Y. T.; Evall, J.; Whitesides, G. M.; Nuzzo, R. G. Formation of Monolayer Films by the Spontaneous Assembly of Organic Thiols from Solution onto Gold. *Journal of the American Chemical Society* **1989,** *111*, 321-335.
7. Love, J. C.; Estroff, L. A.; Kriebel, J. K.; Nuzzo, R. G.; Whitesides, G. M. Self-Assembled Monolayers of Thiolates on Metals as a Form of Nanotechnology. *Chemical Reviews* **2005,** *105*, 1103-1170.
8. Vericat, C.; Vela, M. E.; Benitez, G.; Carro, P.; Salvarezza, R. C. Self-Assembled Monolayers of Thiols and Dithiols on Gold: New Challenges for a Well-Known System. *Chem Soc Rev* **2010,** *39*, 1805-1834.
9. Park, C. S.; Colorado, R.; Jamison, A. C.; Lee, T. R. Thiol-Based Self-Assembled Monolayers: Formation, Organization, and the Role of Adsorbate Structure. In *Reference Module in Materials Science and Materials Engineering*; Elsevier, 2016.
10. Khalid, W.; El Helou, M.; Murböck, T.; Yue, Z.; Montenegro, J.-M.; Schubert, K.; Göbel, G.; Lisdat, F.; Witte, G.; Parak, W. J. Immobilization of Quantum Dots Via Conjugated Self-Assembled Monolayers and Their Application as a Light-Controlled Sensor for the Detection of Hydrogen Peroxide. *ACS Nano* **2011,** *5*, 9870-9876.
11. Niklewski, A.; Azzam, W.; Strunskus, T.; Fischer, R. A.; Wöll, C. Fabrication of Self-Assembled Monolayers Exhibiting a Thiol-Terminated Surface. *Langmuir* **2004,** *20*, 8620-8624.
12. Niskala, J. R.; Rice, W. C.; Bruce, R. C.; Merkel, T. J.; Tsui, F.; You, W. Tunneling Characteristics of Au–Alkanedithiol–Au Junctions Formed Via Nanotransfer Printing (Ntp). *Journal of the American Chemical Society* **2012,** *134*, 12072-12082.
13. Xie, Z.; Bâldea, I.; Smith, C. E.; Wu, Y.; Frisbie, C. D. Experimental and Theoretical Analysis of Nanotransport in Oligophenylene Dithiol Junctions as a Function of Molecular Length and Contact Work Function. *ACS Nano* **2015,** *9*, 8022-8036.
14. Chen, J.-J.; Struk, K. N.; Brennan, A. B. Surface Modification of Silicate Glass Using 3-(Mercaptopropyl)Trimethoxysilane for Thiol–Ene Polymerization. *Langmuir* **2011,** *27*, 13754-13761.
15. Harant, A. W.; Khire, V. S.; Thibodaux, M. S.; Bowman, C. N. Thiol−Ene Photopolymer Grafts on Functionalized Glass and Silicon Surfaces. *Macromolecules* **2006,** *39*, 1461-1466.
16. Li, J.-R.; Lusker, K. L.; Yu, J.-J.; Garno, J. C. Engineering the Spatial Selectivity of Surfaces at the Nanoscale Using Particle Lithography Combined with Vapor Deposition of Organosilanes. *ACS Nano* **2009,** *3*, 2023-2035.
17. Reynolds, N. P.; Tucker, J. D.; Davison, P. A.; Timney, J. A.; Hunter, C. N.; Leggett, G. J. Site-Specific Immobilization and Micrometer and Nanometer Scale Photopatterning of Yellow Fluorescent Protein on Glass Surfaces. *Journal of the American Chemical Society* **2009,** *131*, 896-897.
18. Lud, S. Q.; Neppl, S.; Richter, G.; Bruno, P.; Gruen, D. M.; Jordan, R.; Feulner, P.; Stutzmann, M.; Garrido, J. A. Controlling Surface Functionality through Generation of Thiol Groups in a Self-Assembled Monolayer. *Langmuir* **2010,** *26*, 15895-15900.
19. Esmaeilzadeh, P.; Köwitsch, A.; Liedmann, A.; Menzel, M.; Fuhrmann, B.; Schmidt, G.; Klehm, J.; Groth, T. Stimuli-Responsive Multilayers Based on Thiolated Polysaccharides That Affect Fibroblast Cell Adhesion. *ACS Applied Materials & Interfaces* **2018,** *10*, 8507-8518.
20. Schlenoff, J. B.; Li, M.; Ly, H. Stability and Self-Exchange in Alkanethiol Monolayers. *Journal of the American Chemical Society* **1995,** *117*, 12528-12536.

21. Biggs, C. I.; Walker, M.; Gibson, M. I. "Grafting to" of Rafted Responsive Polymers to Glass Substrates by Thiol–Ene and Critical Comparison to Thiol–Gold Coupling. *Biomacromolecules* **2016,** *17*, 2626-2633.
22. McKenas, C. G.; Fehr, J. M.; Donley, C. L.; Lockett, M. R. Thiol–Ene Modified Amorphous Carbon Substrates: Surface Patterning and Chemically Modified Electrode Preparation. *Langmuir* **2016,** *32*, 10529-10536.
23. Dubacheva, G. V.; Curk, T.; Mognetti, B. M.; Auzély-Velty, R.; Frenkel, D.; Richter, R. P. Superselective Targeting Using Multivalent Polymers. *Journal of the American Chemical Society* **2014,** *136*, 1722-1725.
24. Felgueiras, H. P.; Wang, L. M.; Ren, K. F.; Querido, M. M.; Jin, Q.; Barbosa, M. A.; Ji, J.; Martins, M. C. L. Octadecyl Chains Immobilized onto Hyaluronic Acid Coatings by Thiol–Ene "Click Chemistry" Increase the Surface Antimicrobial Properties and Prevent Platelet Adhesion and Activation to Polyurethane. *ACS Applied Materials & Interfaces* **2017,** *9*, 7979-7989.
25. Li, J.; Li, L.; Du, X.; Feng, W.; Welle, A.; Trapp, O.; Grunze, M.; Hirtz, M.; Levkin, P. A. Reactive Superhydrophobic Surface and Its Photoinduced Disulfide-Ene and Thiol-Ene (Bio)Functionalization. *Nano Letters* **2015,** *15*, 675-681.
26. De Leener, G.; Evoung-Evoung, F.; Lascaux, A.; Mertens, J.; Porras-Gutierrez, A. G.; Le Poul, N.; Lagrost, C.; Over, D.; Leroux, Y. R.; Reniers, F.; Hapiot, P.; Le Mest, Y.; Jabin, I.; Reinaud, O. Immobilization of Monolayers Incorporating Cu Funnel Complexes onto Gold Electrodes. Application to the Selective Electrochemical Recognition of Primary Alkylamines in Water. *Journal of the American Chemical Society* **2016,** *138*, 12841-12853.
27. Kwiat, M.; Elnathan, R.; Kwak, M.; de Vries, J. W.; Pevzner, A.; Engel, Y.; Burstein, L.; Khatchtourints, A.; Lichtenstein, A.; Flaxer, E.; Herrmann, A.; Patolsky, F. Non-Covalent Monolayer-Piercing Anchoring of Lipophilic Nucleic Acids: Preparation, Characterization, and Sensing Applications. *Journal of the American Chemical Society* **2012,** *134*, 280-292.
28. Peng, H.; Wang, C.; Xi, W.; Kowalski, B. A.; Gong, T.; Xie, X.; Wang, W.; Nair, D. P.; McLeod, R. R.; Bowman, C. N. Facile Image Patterning Via Sequential Thiol–Michael/Thiol–Yne Click Reactions. *Chemistry of Materials* **2014,** *26*, 6819-6826.
29. Chelmowski, R.; Köster, S. D.; Kerstan, A.; Prekelt, A.; Grunwald, C.; Winkler, T.; Metzler-Nolte, N.; Terfort, A.; Wöll, C. Peptide-Based Sams That Resist the Adsorption of Proteins. *Journal of the American Chemical Society* **2008,** *130*, 14952-14953.
30. Devaraj, N. K.; Miller, G. P.; Ebina, W.; Kakaradov, B.; Collman, J. P.; Kool, E. T.; Chidsey, C. E. D. Chemoselective Covalent Coupling of Oligonucleotide Probes to Self-Assembled Monolayers. *Journal of the American Chemical Society* **2005,** *127*, 8600-8601.
31. Gevrek, T. N.; Kosif, I.; Sanyal, A. Surface-Anchored Thiol-Reactive Soft Interfaces: Engineering Effective Platforms for Biomolecular Immobilization and Sensing. *ACS Applied Materials & Interfaces* **2017,** *9*, 27946-27954.
32. Robin, M. P.; Wilson, P.; Mabire, A. B.; Kiviaho, J. K.; Raymond, J. E.; Haddleton, D. M.; O'Reilly, R. K. Conjugation-Induced Fluorescent Labeling of Proteins and Polymers Using Dithiomaleimides. *Journal of the American Chemical Society* **2013,** *135*, 2875-2878.
33. Wasserberg, D.; Nicosia, C.; Tromp, E. E.; Subramaniam, V.; Huskens, J.; Jonkheijm, P. Oriented Protein Immobilization Using Covalent and Noncovalent Chemistry on a Thiol-Reactive Self-Reporting Surface. *Journal of the American Chemical Society* **2013,** *135*, 3104-3111.

34. Zhang, Y.; Zhou, X.; Xie, Y.; Greenberg, M. M.; Xi, Z.; Zhou, C. Thiol Specific and Tracelessly Removable Bioconjugation Via Michael Addition to 5-Methylene Pyrrolones. *Journal of the American Chemical Society* **2017,** *139*, 6146-6151.
35. Houseman, B. T.; Gawalt, E. S.; Mrksich, M. Maleimide-Functionalized Self-Assembled Monolayers for the Preparation of Peptide and Carbohydrate Biochips. *Langmuir* **2003,** *19*, 1522-1531.
36. MacBeath, G.; Koehler, A. N.; Schreiber, S. L. Printing Small Molecules as Microarrays and Detecting Protein−Ligand Interactions En Masse. *Journal of the American Chemical Society* **1999,** *121*, 7967-7968.
37. Gribova, V.; Gauthier-Rouvière, C.; Albigès-Rizo, C.; Auzely-Velty, R.; Picart, C. Effect of Rgd Functionalization and Stiffness Modulation of Polyelectrolyte Multilayer Films on Muscle Cell Differentiation. *Acta Biomaterialia* **2013,** *9*, 6468-6480.
38. Roberts, J. N.; Sahoo, J. K.; McNamara, L. E.; Burgess, K. V.; Yang, J.; Alakpa, E. V.; Anderson, H. J.; Hay, J.; Turner, L.-A.; Yarwood, S. J.; Zelzer, M.; Oreffo, R. O. C.; Ulijn, R. V.; Dalby, M. J. Dynamic Surfaces for the Study of Mesenchymal Stem Cell Growth through Adhesion Regulation. *ACS Nano* **2016,** *10*, 6667-6679.
39. Thompson, M. T.; Berg, M. C.; Tobias, I. S.; Lichter, J. A.; Rubner, M. F.; Van Vliet, K. J. Biochemical Functionalization of Polymeric Cell Substrata Can Alter Mechanical Compliance. *Biomacromolecules* **2006,** *7*, 1990-1995.
40. Davila, J.; Chassepot, A.; Longo, J.; Boulmedais, F.; Reisch, A.; Frisch, B.; Meyer, F.; Voegel, J.-C.; Mésini, P. J.; Senger, B.; Metz-Boutigue, M.-H.; Hemmerlé, J.; Lavalle, P.; Schaaf, P.; Jierry, L. Cyto-Mechanoresponsive Polyelectrolyte Multilayer Films. *Journal of the American Chemical Society* **2012,** *134*, 83-86.
41. Picart, C.; Elkaim, R.; Richert, L.; Audoin, F.; Arntz, Y.; Da Silva Cardoso, M.; Schaaf, P.; Voegel, J. C.; Frisch, B. Primary Cell Adhesion on Rgd-Functionalized and Covalently Crosslinked Thin Polyelectrolyte Multilayer Films. *Advanced Functional Materials* **2005,** *15*, 83-94.
42. Carro, P.; Creus, A. H.; Muñoz, A.; Salvarezza, R. C. On the Thermodynamic Stability of A,Ω-Alkanedithiols Self-Assembled Monolayers on Unreconstructed and Reconstructed Au(111). *Langmuir* **2010,** *26*, 9589-9595.
43. Hamoudi, H.; Esaulov, V. A. Selfassembly of A,Ω-Dithiols on Surfaces and Metal Dithiol Heterostructures. *Annalen der Physik* **2016,** *528*, 242-263.
44. Tostanoski, L. H.; Chiu, Y.-C.; Andorko, J. I.; Guo, M.; Zeng, X.; Zhang, P.; Royal, W.; Jewell, C. M. Design of Polyelectrolyte Multilayers to Promote Immunological Tolerance. *ACS Nano* **2016,** *10*, 9334-9345.
45. Salloum, D. S.; Schlenoff, J. B. Protein Adsorption Modalities on Polyelectrolyte Multilayers. *Biomacromolecules* **2004,** *5*, 1089-1096.
46. Su, X.; Kim, B.-S.; Kim, S. R.; Hammond, P. T.; Irvine, D. J. Layer-by-Layer-Assembled Multilayer Films for Transcutaneous Drug and Vaccine Delivery. *ACS Nano* **2009,** *3*, 3719-3729.
47. Zhang, P.; Chiu, Y.-C.; Tostanoski, L. H.; Jewell, C. M. Polyelectrolyte Multilayers Assembled Entirely from Immune Signals on Gold Nanoparticle Templates Promote Antigen-Specific T Cell Response. *ACS Nano* **2015,** *9*, 6465-6477.
48. Ghostine, R. A.; Markarian, M. Z.; Schlenoff, J. B. Asymmetric Growth in Polyelectrolyte Multilayers. *Journal of the American Chemical Society* **2013,** *135*, 7636-7646.
49. Schlenoff, J. B.; Dubas, S. T. Mechanism of Polyelectrolyte Multilayer Growth: Charge Overcompensation and Distribution. *Macromolecules* **2001,** *34*, 592-598.

50. Salloum, D. S.; Olenych, S. G.; Keller, T. C. S.; Schlenoff, J. B. Vascular Smooth Muscle Cells on Polyelectrolyte Multilayers: Hydrophobicity-Directed Adhesion and Growth. *Biomacromolecules* **2005,** *6*, 161-167.
51. Schlenoff, J. B.; Rmaile, A. H.; Bucur, C. B. Hydration Contributions to Association in Polyelectrolyte Multilayers and Complexes: Visualizing Hydrophobicity. *Journal of the American Chemical Society* **2008,** *130*, 13589-13597.
52. Yoo, P. J.; Zacharia, N. S.; Doh, J.; Nam, K. T.; Belcher, A. M.; Hammond, P. T. Controlling Surface Mobility in Interdiffusing Polyelectrolyte Multilayers. *ACS Nano* **2008,** *2*, 561-571.
53. Arias, C. J.; Surmaitis, R. L.; Schlenoff, J. B. Cell Adhesion and Proliferation on the "Living" Surface of a Polyelectrolyte Multilayer. *Langmuir* **2016,** *32*, 5412-5421.
54. Schlenoff, J. B.; Dharia, J. R.; Xu, H.; Wen, L.; Li, M. Adsorption of Thiol-Containing Copolymers onto Gold. *Macromolecules* **1995,** *28*, 4290-4295.
55. Euti, E. M.; Vélez-Romero, P.; Leiva, E. P. M.; Macagno, V. A.; Paredes-Olivera, P. A.; Patrito, E. M.; Cometto, F. P. The Role of Tris(2-Carboxyethyl)Phosphine Reducing Agent in the Controlled Formation of A,Ω-Alkanedithiols Monolayers on Au(111) with Monocoordinated and Bicoordinated Configurations. *Langmuir* **2016,** *32*, 9428-9436.
56. Gronowicz, G. A.; Derome, M. E. Synthetic Peptide Containing Arg-Gly-Asp Inhibits Bone Formation and Resorption in a Mineralizing Organ Culture System of Fetal Rat Parietal Bones. *Journal of Bone and Mineral Research* **1994,** *9*, 193-201.
57. Arias, C. J.; Keller, T. C. S.; Schlenoff, J. B. Quasi-Spherical Cell Clusters Induced by a Polyelectrolyte Multilayer. *Langmuir* **2015,** *31*, 6436-6446.
58. Ruoslahti, E.; Öbrink, B. Common Principles in Cell Adhesion. *Experimental Cell Research* **1996,** *227*, 1-11.
59. Plow, E. F.; Haas, T. A.; Zhang, L.; Loftus, J.; Smith, J. W. Ligand Binding to Integrins. *Journal of Biological Chemistry* **2000,** *275*, 21785-21788.
60. Tsai, W.-B.; Chen, R. P.-Y.; Wei, K.-L.; Chen, Y.-R.; Liao, T.-Y.; Liu, H.-L.; Lai, J.-Y. Polyelectrolyte Multilayer Films Functionalized with Peptides for Promoting Osteoblast Functions. *Acta Biomaterialia* **2009,** *5*, 3467-3477.
61. Berg, M. C.; Yang, S. Y.; Hammond, P. T.; Rubner, M. F. Controlling Mammalian Cell Interactions on Patterned Polyelectrolyte Multilayer Surfaces. *Langmuir* **2004,** *20*, 1362-1368.
62. Tsai, W.-B.; Chen, R. P.-Y.; Wei, K.-L.; Tan, S.-F.; Lai, J.-Y. Modulation of Rgd-Functionalized Polyelectrolyte Multilayer Membranes for Promoting Osteoblast Function. *Journal of Biomaterials Science, Polymer Edition* **2010,** *21*, 377-394.
63. Massia, S. P.; Hubbell, J. A. An Rgd Spacing of 440 Nm Is Sufficient for Integrin Alpha V Beta 3-Mediated Fibroblast Spreading and 140 Nm for Focal Contact and Stress Fiber Formation. *The Journal of Cell Biology* **1991,** *114*, 1089.
64. Rajagopalan, P.; Marganski, W. A.; Brown, X. Q.; Wong, J. Y. Direct Comparison of the Spread Area, Contractility, and Migration of Balb/C 3t3 Fibroblasts Adhered to Fibronectin- and Rgd-Modified Substrata. *Biophysical Journal* **2004,** *87*, 2818-2827.
65. Boulmedais, F.; Frisch, B.; Etienne, O.; Lavalle, P.; Picart, C.; Ogier, J.; Voegel, J. C.; Schaaf, P.; Egles, C. Polyelectrolyte Multilayer Films with Pegylated Polypeptides as a New Type of Anti-Microbial Protection for Biomaterials. *Biomaterials* **2004,** *25*, 2003-2011.
66. Wilson, J. T.; Cui, W.; Kozlovskaya, V.; Kharlampieva, E.; Pan, D.; Qu, Z.; Krishnamurthy, V. R.; Mets, J.; Kumar, V.; Wen, J.; Song, Y.; Tsukruk, V. V.; Chaikof, E. L.

Cell Surface Engineering with Polyelectrolyte Multilayer Thin Films. *Journal of the American Chemical Society* **2011,** *133*, 7054-7064.
67. Cortez, C.; Quinn, J. F.; Hao, X.; Gudipati, C. S.; Stenzel, M. H.; Davis, T. P.; Caruso, F. Multilayer Buildup and Biofouling Characteristics of Pss-B-Peg Containing Films. *Langmuir* **2010,** *26*, 9720-9727.
68. Harder, P.; Grunze, M.; Dahint, R.; Whitesides, G. M.; Laibinis, P. E. Molecular Conformation in Oligo(Ethylene Glycol)-Terminated Self-Assembled Monolayers on Gold and Silver Surfaces Determines Their Ability to Resist Protein Adsorption. *The Journal of Physical Chemistry B* **1998,** *102*, 426-436.
69. Jomaa, H. W.; Schlenoff, J. B. Salt-Induced Polyelectrolyte Interdiffusion in Multilayered Films: A Neutron Reflectivity Study. *Macromolecules* **2005,** *38*, 8473-8480.
70. Fu, J.; Fares, H. M.; Schlenoff, J. B. Ion-Pairing Strength in Polyelectrolyte Complexes. *Macromolecules* **2017,** *50*, 1066-1074.
71. Nath, N.; Chilkoti, A. Label-Free Biosensing by Surface Plasmon Resonance of Nanoparticles on Glass: Optimization of Nanoparticle Size. *Analytical Chemistry* **2004,** *76*, 5370-5378.
72. Saha, K.; Agasti, S. S.; Kim, C.; Li, X.; Rotello, V. M. Gold Nanoparticles in Chemical and Biological Sensing. *Chemical Reviews* **2012,** *112*, 2739-2779.
73. Sepúlveda, B.; Angelomé, P. C.; Lechuga, L. M.; Liz-Marzán, L. M. Lspr-Based Nanobiosensors. *Nano Today* **2009,** *4*, 244-251.
74. Fan, M.; Andrade, G. F. S.; Brolo, A. G. A Review on the Fabrication of Substrates for Surface Enhanced Raman Spectroscopy and Their Applications in Analytical Chemistry. *Analytica Chimica Acta* **2011,** *693*, 7-25.
75. Stewart, M. E.; Anderton, C. R.; Thompson, L. B.; Maria, J.; Gray, S. K.; Rogers, J. A.; Nuzzo, R. G. Nanostructured Plasmonic Sensors. *Chemical Reviews* **2008,** *108*, 494-521.
76. Toderas, F.; Baia, M.; Baia, L.; Astilean, S. Controlling Gold Nanoparticle Assemblies for Efficient Surface-Enhanced Raman Scattering and Localized Surface Plasmon Resonance Sensors. *Nanotechnology* **2007,** *18*, 255702.
77. Jiang, X. P.; Zheng, H. P.; Gourdin, S.; Hammond, P. T. Polymer-on-Polymer Stamping: Universal Approaches to Chemically Patterned Surfaces. *Langmuir* **2002,** *18*, 2607-2615.
78. Goss, C. A.; Charych, D. H.; Majda, M. Application of (3-Mercaptopropyl)Trimethoxysilane as a Molecular Adhesive in the Fabrication of Vapor-Deposited Gold Electrodes on Glass Substrates. *Analytical Chemistry* **1991,** *63*, 85-88.
79. Turkevich, J.; Stevenson, P. C.; Hillier, J. A Study of the Nucleation and Growth Processes in the Synthesis of Colloidal Gold. *Discussions of the Faraday Society* **1951,** *11*, 55-75.

REVISED

Table of Contents Graphic FOR PUBLICATION ONLY